# Stabilization of Domain Walls between Traveling Waves by Nonlinear Mode Coupling in Taylor-Couette Flow

M. Heise,[1] Ch. Hoffmann,[2] J. Abshagen,[1] A. Pinter,[2] G. Pfister,[1] and M. Lücke[2]

[1]*Institut für Experimentelle und Angewandte Physik, Universität Kiel, D-24098 Kiel, Germany*
[2]*Institut für Theoretische Physik, Universität des Saarlandes, D-66041 Saarbrücken, Germany*

(Received 30 March 2007; published 12 February 2008)

We present a new mechanism that allows the stable existence of domain walls between oppositely traveling waves in pattern-forming systems far from onset. It involves a nonlinear mode coupling that results directly from the nonlinearities in the underlying momentum balance. Our work provides the first observation and explanation of such strongly nonlinearly driven domain walls that separate structured states by a phase generating or annihilating defect. Furthermore, the influence of a symmetry breaking externally imposed flow on the wave domains and the domain walls is studied. The results are obtained for vortex waves in the Taylor-Couette system by combining numerical simulations of the full Navier-Stokes equations and experimental measurements.

DOI: 10.1103/PhysRevLett.100.064501 PACS numbers: 47.20.Ky, 02.30.Oz, 05.45.−a

Structured states appear spontaneously as a result of a pattern-forming instability in a large variety of driven nonequilibrium systems, e.g., in optics, chemical and biological models, polymer and binary mixtures, liquid crystals, convection, and shear flow [1–3]. However, these patterns are seldom globally ordered. Rather, there exist patches, i.e., spatial domains with different order parameters or symmetries of the structures. The formation of such domains and their interaction via domain walls has often been investigated close to onset. Then the amplitudes of the order-parameter fields are small and slowly varying and the spatiotemporal behavior of the system can be modeled with Ginzburg-Landau equations (GLE).

Simple examples are 1D patterns of oppositely traveling waves (TWs) [3–6] that appear, e.g., via a forward Hopf bifurcation in systems with spatial translation and reflection symmetry. Also the domain walls between two such TWs, i.e., their sources or sinks, are close to onset well described by coupled GLE for the slowly varying amplitudes of the two critical TW modes [7,8]—see, however, the deviations at a larger distance from threshold in [4]. On the other hand, 2D patterns allow defects and domains with more complex spatiotemporal behavior. However, coupled GLE or order-parameter equations that are based on the critical modes of the patterns in question have been used successfully also for these systems to model various aspects of their behavior [1–3,9–12].

Here we elucidate how walls separating domains of waves that travel into opposite directions appear far from onset by a strongly nonlinear balance of generalized forces. This balance is dominated by a nonlinear mode coupling that involves not only the two critical TW modes but, in addition, also a third, stationary one, with different spatial symmetry. Our investigation is performed in a Taylor-Couette system since it allows quantitative comparisons between experiment and numerical simulation of the full Navier-Stokes equations (NSE) well beyond the first instability and also in the case of open flow.

*System.*—The system consists of two concentric counterrotating cylinders (inner, outer radius $r_{1,2}$; angular velocities $\Omega_{1,2}$) with a fluid of kinematic viscosity $\nu$ in the gap between them. Lengths are scaled by the gap width $d = r_2 - r_1$, velocities by $\nu/d$, and time by the diffusion time $\tau = d^2/\nu$. For numerical calculations of the velocity field $\mathbf{u} = u\mathbf{e}_r + v\mathbf{e}_\varphi + w\mathbf{e}_z$, which is governed by the

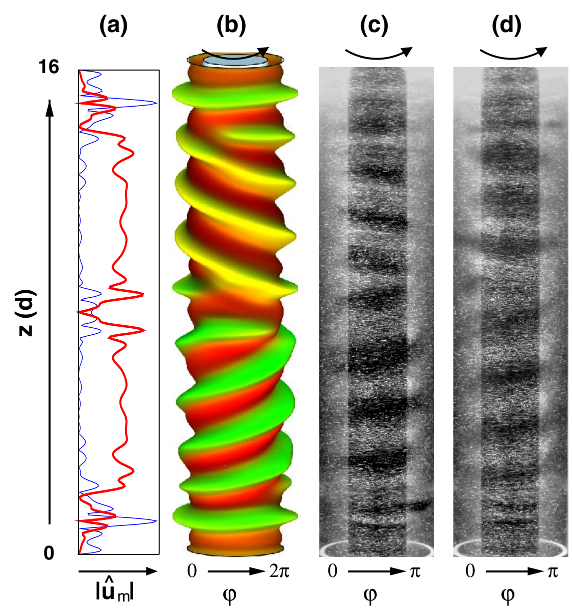


FIG. 1 (color online). Visualization of a stable $P_+$ state in a finite system: (a) azimuthal Fourier amplitudes $|\hat{u}_m(z)|$ for $m = 0$ [thin (blue) line] and $m = 1$ [thick (red) line] at midgap; (b) 3D visualization of $u(\varphi, z)$ at midgap (for visibility, the whole $2\pi$ cylinder is displayed); (c),(d) two successive photographs of this state in experiment. Parameters are $R_1 = 140$ and Re $= 0$.

 

NSE, a combined Galerkin and finite difference code is used as described in [13]. In the experimental setup the cylinder radii are $r_1 = (12.50 \pm 0.01)$ mm and $r_2 = (25.00 \pm 0.01)$ mm. For measurements we used flow visualization and laser Doppler velocimetry (LDV) as described in detail in [14]. Control parameters are the inner and outer cylinder Reynolds numbers $R_{1,2} = r_{1,2}\Omega_{1,2}d/\nu$ and the Reynolds number Re of the externally imposed throughflow, which is given by the mean axial velocity $\langle w \rangle$ (averaged over the annular cross section). In this Letter, the radius ratio $\eta = r_1/r_2 = 0.5$, the aspect ratio $\Gamma = 16$, and $R_2 = -125$ are held constant.

*Bifurcation behavior and domains.*—For axially periodic boundary conditions and sufficiently large $R_1$, the laminar Couette-Poiseuille flow (CPF) undergoes a transition to azimuthally rotating and axially traveling open spiral vortices. Two types of such spiral TWs exist: left-handed spirals (L-SPI) and right-handed spirals (R-SPI). For Re $= 0$ they bifurcate forward out of the basic CPF at $R_1 = 117.2$ and neither of the two spiral types is preferred; i.e., the initially selected type remains stable [13]. An externally imposed axial throughflow breaks the axial mirror symmetry and shifts the stability thresholds of the spirals depending on their chirality [13,14].

When the system is axially bounded by rigid nonrotating lids, there appear axisymmetric, toroidally closed Ekman vortices close to these lids with amplitudes that decay roughly exponentially into the bulk. Then spirals can occupy a bulk region that is delimited by two rotating defects [15]. Each of them is located adjacent to the respective Ekman vortex structure. These defects generate or annihilate the phase of the spirals in the bulk. The spatiotemporal properties of these global spirals extending over the whole bulk region between the rotating end defects are for sufficiently large systems, as the one investigated here, similar to axially periodic systems [14,15].

However, for rigid boundaries we found—in contrast to periodic ones—that the above described stable global SPI states can undergo a transition to a new stable state as $R_1$ is increased. This new state consists of two localized spirals with different chirality: e.g., an upward traveling L-SPI in the upper and a downward traveling R-SPI in the lower half of the bulk being separated by a defect. After transients have died out, this defect between the two TWs does not propagate in axial direction and the flow state rotates stationarily as a whole.

Plots of this flow state based on numerical calculations and photographs of the experiment are shown in Fig. 1. A snapshot in 1(b) visualizes the numerically obtained radial velocity field $u$ over the whole $2\pi$ range of a cylinder surface at radial midgap. Amplitude profiles of the axisymmetric mode $|\hat{u}_{m=0}|$ and of the spiral mode $|\hat{u}_{m=1}|$ of $u$ at midgap are plotted in Fig. 1(a) ($m$ denotes the azimuthal wave number of the respective mode). Figures 1(c) and 1(d) give two successive flow visualization snapshots of this state in experiment, each presenting a half-cylinder surface.

*Defects and notation.*—Since phase is generated in the defect of Fig. 1, we call it a $P_+$ defect. It separates two domains of spirals with different chirality, namely, a L-SPI in the upper and a R-SPI in the lower part of the system. Furthermore, we call the whole flow in such a configuration a $P_+$ state for short. The phase that is generated in a $P_+$ defect in the bulk is annihilated in Ekman-spiral defects near the lids. In this Letter we discuss mainly this flow state, but we also observed $P_-$ states with phase generating Ekman-spiral defects and a phase annihilating defect in the bulk. We found that real and imaginary parts of the complex spiral amplitude $\hat{u}_{m=1}$ vanish at each time in the $P_\pm$ defect as well as in the Ekman-spiral defects; i.e., they are of Ising type (as observed, e.g., in nematic liquid crystals or reaction diffusion systems [16–18]).

The crucial difference between the defect of this *new* $P_+$ state depicted in Fig. 1 and a plain superposition of fronts of two critical, counterpropagating TW modes as in "classic" sinks or sources [8] is the coupling to a finite, nonlinearly driven $m = 0$ mode. The amplitude profile of this mode near the defect can be seen from Fig. 1(a). Note that the latter being rotational symmetric and stationary displays different spatiotemporal behavior than the two critical spiral TW modes. The local axial wave number of this $m = 0$ vortex structure is about twice that of the spirals, and its amplitude grows proportional to the product of the spiral amplitudes. This is easily seen to be a consequence of the Reynolds stresses that, e.g., the critical spiral modes exert on the $m = 0$ flow in the defect region. Close to onset, we did not find stable $P_\pm$ states since the amplitudes of the two SPI modes need to reach a sufficient strength to generate a stabilizing $m = 0$ mode via nonlinear coupling.

The $P_\pm$ states do not require the presence of lid generated Ekman vortices since $P_\pm$ defects exist also in periodic systems. This we have numerically verified in simulations of long systems with axially periodic boundary conditions. In this case, the flow contains a stable pair of a phase generating $P_+$ and a phase annihilating $P_-$ defect, which partition the axial periodicity interval into a L-SPI and a R-SPI domain. At each of the two domain walls the nonlinearly driven $m = 0$ mode appears as in rigidly bounded annuli with a magnitude that is comparable to the spiral mode's amplitudes away from the defect. Furthermore, this state is stable—the axial distance between the two defects remains constant.

*Spatiotemporal development of domains.*—Starting with a global spiral in the bulk as the initial condition and increasing $R_1$ beyond a certain threshold, domains of localized spirals with different chirality usually appear when an Ekman-spiral defect splits up into two defects. The new one then propagates into the global spiral state, thereby unfolding a domain of opposite chirality. We found that the transitions between different global and localized spirals are initiated by such propagating defects. These defects either travel the whole way toward the other lid or they stop at a fixed axial position inside the bulk depending on Re and $R_1$. The latter scenario is documented in Fig. 2. We start [left side of Fig. 2(a)] with an upward propagating global L-SPI for $R_1 = 140$. This lies slightly above the transition threshold to $P_+$ states so that the system evolves into a stable $P_+$ state. First, a wavylike disturbance grows near the bottom lid, which propagates into the bulk, and the phase generating Ekman-spiral defect changes thereby to a phase annihilating one. Then, the $P_+$ defect travels up to its final position at midheight of the system. This final (stable) state is temporally expanded in Fig. 2(b). Furthermore, we found numerically that only phase differences of $\alpha = \pi$ or 0 between the spiral TWs are stable. Initial states with other $\alpha$ values undergo a transition to defects with either $\alpha = \pi$ or $\alpha = 0$.

Figures 2(c)–2(e) show experimental time series of the axial velocity $w(z(t), t)$ that are recorded by moving the LDV measurement spot at fixed $r = r_1 + 0.11d$ and $\varphi$ with constant velocity $w_{\mathrm{LDV}}$ along the path $z(t) = w_{\mathrm{LDV}}t$. The plots represent the flow before 2(c) and after 2(d) the appearance of the defect and the final $P_+$ state 2(e). Thin lines refer to regions where $w$ is basically constant in time. In the spiral regions, on the other hand, many oscillation periods of $w$ are monitored with the small axial scan

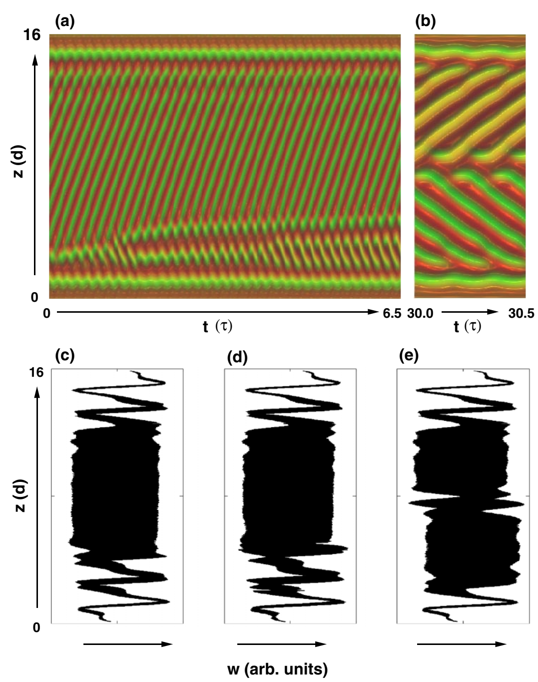


FIG. 2 (color online). Spatiotemporal behavior of a $P_+$ defect propagating into a global L-SPI: (a),(b) numerically simulated radial velocity field $u(z, t)$ at midgap, (a) appearance near the lower lid and upward propagation, (b) final state including the $P_+$ defect; (c)–(e) temporal evolution of this state measured by axial scans of (c) $w$ before and (d) after the defect appearance and (e) final $P_+$ state. Parameters are $R_1 = 140$ and Re $= 0$.

velocity of $w_{\mathrm{LDV}} = 0.16d/\tau$. Thus, the experimental signal appears there, within the resolution of Figs. 2(c)–2(e), as a broad black band.

*Throughflow.*—Starting from a stable $P_+$ state as initial state and switching on external throughflow instantaneously, the $P_+$ defect begins to propagate downstream. Thereby the R-SPI domain expands. The initial propagation velocity $w_d$ of this defect is illustrated in Fig. 3 showing experimental (△) and numerical (▲) results. As expected, $w_d$ is proportional to Re, i.e., to the mean axial flow. In the vicinity of a bulk $P_+$ defect, all Fourier modes $|\hat{\mathbf{u}}_m|$ are constant in time in an axially with $w_d$ comoving frame.

Numerical simulations showed that the velocity $w_d$ decreases when the defect approaches an axial end and, for small throughflow (Re $< 0.2$), it stops at a certain axial position inside the bulk, since the stationary Ekman structure becomes more dominant near the lids. Only sufficiently large throughflow (Re $> 0.2$) is able to "blow" the defect out of the bulk. In that case, the final structure is a global R-SPI.

*Phase diagram.*—Imposing an external axial throughflow (which is vaguely analogous to applying an external magnetic field in the case of magnetic domains) breaks the symmetry degeneracy of the SPI solution. Hence, the Hopf bifurcation to spirals splits up into a branch of downstream propagating L-SPI, which bifurcates first, and into a branch of upstream propagating R-SPI, which bifurcates at a larger $R_1$. Furthermore, the phase velocities of both spirals are changed [13,14].

The numerically determined bifurcation thresholds of L-SPI and R-SPI for periodic boundary conditions are marked as a single thick line in Fig. 4 since the small difference is not distinguishable for this resolution. It is almost identical to the absolute instability threshold of L-SPI for the control parameter regime considered here. For positive throughflow, the bifurcation as well as the absolute instability threshold for R-SPI lie slightly above those of L-SPI but are not distinguishable from them for the resolution in this figure [14,19].

Only stable states are depicted in the phase diagram of Fig. 4; open (closed) symbols refer to experimental (numerical) results. Stability boundaries were mostly deter-

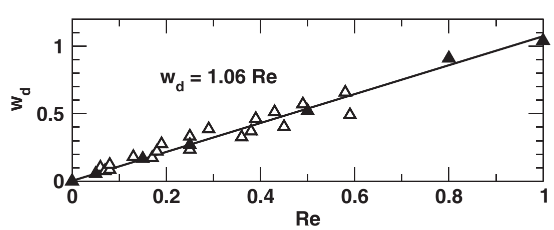


FIG. 3. Experimental (△) and numerical (▲) axial propagation velocity $w_d$ of a $P_+$ defect versus Re. Symbols describe its velocity at midheight of the system for $R_1 = 140$. The line is a linear fit.

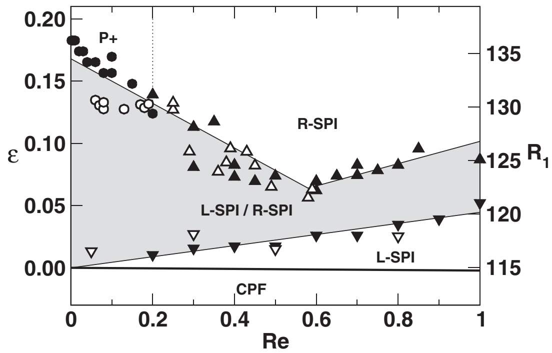


FIG. 4. Phase diagram of CPF, L-SPI, R-SPI, and $P_+$ states. Open (closed) symbols denote experimental (numerical) results. Stability regions are separated by thin lines to guide the eyes. Upward (downward) oriented triangles identify transitions from global L-SPI to global R-SPI (R-SPI to L-SPI), and circles a transition from global L-SPI or R-SPI to stable $P_+$ states. The vertical dotted thin line roughly indicates a boundary between $P_+$ and global R-SPI states. The bottom solid, nearly horizontal line represents the bifurcation threshold for SPI. In the range of Re shown here, the thresholds for both spiral types fall together for the given resolution. $\epsilon = R_1/R_{1,c} - 1$ with $R_{1,c} = 115$ ($R_{1,c} = 117.2$) in experiment (numerical) calculations. The $R_1$ axis is based on the experimental $R_{1,c}$.

mined by varying $R_1$ quasistatically at fixed Re. However, also selected Re scans at fixed $R_1$ were done. For control parameters in the shaded region, global L-SPI and global R-SPI are bistable. The global R-SPI state loses stability below the line marked by (▽, ▼) and undergoes a transition to the global L-SPI state. Hence, for small $R_1$, the system prefers that spiral type, which is traveling downstream as in axially periodic systems [13]. On the other hand, above the line marked by (△, ▲) the global L-SPI state undergoes a transition to a global R-SPI (for Re $\gtrsim$ 0.2). In both cases the chirality of the spirals is changed via a transient in which a $P_+$ (L-SPI to R-SPI) or a $P_-$ defect (R-SPI to L-SPI) is generated at the lower Ekman-spiral defect and then propagates downstream. In fact, the $P_+$ ($P_-$) defect always evolves out of the phase generating (annihilating) Ekman-spiral defect, as described above.

For Re = 0, the two mirror-symmetric global spiral states both undergo a transition to a $P_+$ state with the $P_+$ defect at midheight when the driving is increased (quasistatically) beyond $\epsilon = 0.17$; cf. Fig. 4. With this protocol we have observed neither $P_-$ defects nor $P_-$ states for these parameters. This transition occurs when the phase generating Ekman-spiral defect bounding the global L-SPI (R-SPI) at the lower (upper) end emits a $P_+$ defect that then moves into the center of the system.

For $0 < \mathrm{Re} \lesssim 0.2$ and sufficiently large $\epsilon$ the throughflow is too small to blow such a $P_+$ defect out of the system to induce a transition to a global R-SPI. Instead, the $P_+$ defect moves here after its generation up- or downstream (depending on the initial spiral type) away from the ends into the bulk and remains there. This gives rise to stable but typically asymmetric $P_+$ states above the line marked by (∘, •).

*Conclusion.*—A combined experimental and numerical study has revealed far away from onset the spatiotemporal and bifurcation behavior of nonlinearly driven domain walls between oppositely traveling spiral waves of different chirality. The extended states are separated by phase generating or annihilating defects—both of Ising type. The oppositely traveling spirals drive by nonlinear mode interaction within the domain wall a localized, stationary, rotationally symmetric vortex mode. This nonlinear mode coupling is a characteristic feature of the domain wall and is essential for its robust existence. So, separated domains of oppositely traveling waves can coexist stably in pattern-forming systems even far from onset due to strong nonlinear interactions.

We acknowledge support from the Deutsche Forschungsgemeinschaft.


[1] A. Joets and R. Ribotta, J. Stat. Phys. **64**, 981 (1991).
[2] E. Bodenschatz, W. Pesch, and G. Ahlers, Annu. Rev. Fluid Mech. **32**, 709 (2000).
[3] M. Cross and P. Hohenberg, Rev. Mod. Phys. **65**, 851 (1993).
[4] P. Habdas, M. Case, and J. de Bruyn, Phys. Rev. E **63**, 066305 (2001).
[5] L. Pastur, M.-T. Westra, D. Snouck, W. van de Water, M. van Hecke, C. Storm, and W. van Saarloos, Phys. Rev. E **67**, 036305 (2003).
[6] A. Ezersky, N. Latrache, O. Crumeyrolle, and I. Mutabazi, Theor. Comput. Fluid Dyn. **18**, 85 (2004).
[7] P. Coullet, T. Frisch, and F. Plaza, Physica (Amsterdam) **62D**, 75 (1993).
[8] M. van Hecke, C. Strom, and W. van Saarloos, Physica (Amsterdam) **134D**, 1 (1999).
[9] A. Newell, T. Passot, and J. Lega, Annu. Rev. Fluid Mech. **25**, 399 (1993).
[10] C. Aegerter and C. Surko, Phys. Rev. E **63**, 046301 (2001).
[11] I. S. Aranson and L. Kramer, Rev. Mod. Phys. **74**, 99 (2002).
[12] S. Madruga, H. Riecke, and W. Pesch, Phys. Rev. Lett. **96**, 074501 (2006).
[13] C. Hoffmann, M. Lücke, and A. Pinter, Phys. Rev. E **69**, 056309 (2004).
[14] J. Abshagen, M. Heise, J. Langenberg, and G. Pfister, Phys. Rev. E **75**, 016309 (2007).
[15] C. Hoffmann, M. Lücke, and A. Pinter, Phys. Rev. E **72**, 056311 (2005).
[16] W. Helfrich, Phys. Rev. Lett. **21**, 1518 (1968).
[17] P. Coullet, J. Lega, B. Houchmanzadeh, and J. Lajzerowicz, Phys. Rev. Lett. **65**, 1352 (1990).
[18] A. Hagberg and E. Meron, Phys. Rev. E **48**, 705 (1993).
[19] A. Pinter, M. Lücke, and C. Hoffmann, Phys. Rev. E **67**, 026318 (2003).